Simulation of radiation effects on $In_{0.52}Al_{0.48}As$ and $In_{0.53}Ga_{0.47}As$ by low energy He ion

H. Y. Mei[a], S. H. Zhao[a], Y. Z. Wu[b], P. Zhang[a], H. T. Wu[a], R. X. Yao[a], X. Y. Zheng[a], H. Wen[a] , S. X. Sun[a,c,*]

[a]*Henan Provincial Key Laboratory of Smart Lighting, School of Information Engineering, Huanghuai University, Zhumadian 463000, China*

[b]*School of Information Engineering, Shenyang University, Shenyang 110044, Chna*

[C]*Henan International Joint Laboratory of Behavior Optimization Control for Smart Robots, Zhumadian 463000, China*

In this article, influence of He ions irradiation on $In_{0.52}Al_{0.48}As$ and $In_{0.53}Ga_{0.47}As$ materials with the energies ranging from 50 to 200 keV at normal incidence, including the distributions of the He ions, ionizing energy loss, vacancy, and backscattering ion number, is studied through the simulation. The calculated results show that the peak position of He ion distribution moves to the deeper depth with increasing incident energy and the distribution curve conforms to Bragg distribution. The distribution of the ionizing energy loss induced by He ions is almost constant first and then sharply drops with increasing energy induced by recoil atoms conforms to Bragg distribution. The numbers of vacancies increase with increasing energy and the As vacancy is the prominent vacancy for these two materials. The number of phonons induced by recoil atoms is much higher than that induced by the He ions. The total numbers of the backscattering for the $In_{0.52}Al_{0.48}As$ and $In_{0.53}Ga_{0.47}As$ all decline as the energy is increases and the value for InGaAs is always higher than that the He ions. The higher numbers of backscattering ions are obtained for InAlAs.

(Received March 1, 2022; Accepted July 8, 2022)

Keywords: $In_{0.52}Al_{0.48}As$ and $In_{0.53}Ga_{0.47}As$, He ion, Ionizing energy loss, Phonons distribution

1. Introduction

Because of the high carrier mobility, high breakdown electric field, wide band gap, high thermal and chemical stability characteristics for the III-V compound semiconductor materials[1-4], it is ideally suitable for high power devices and high frequency devices applications, such as high-electron-mobility transistor (HEMT), power metal-oxide -semiconductor field effect transistor (P-MOSFET), Schottky barrier diodes (SBD) etc.,[5-7]. With

* Corresponding authors: sunshuxianga@126.com

https://doi.org/10.15251/DJNB.2022.173.749

the development of fabrication technologies and novel device structures, the frequency characteristics of devices with III-V compound semiconductor materials have made great progress. For HEMT, the maximum oscillation frequency reaches over 1 THz[8]. Therefore, they are widely employed in telecommunication, space, and astronomy science.

When semiconductor devices are applied in space radiation environment, the radiation damage induced by charged ions must be considered[9,10]. The interaction between ions and those III-V compound semiconductors can markedly reduce carrier concentration and mobility because of the carrier removal effect and scattering effect, and thus weaken the device performance, ultimately shorten the orbital service time of the space equipment[11]. In space radiation environment, heavy ions, which comes from the galactic cosmic and solar flares, are main source that affect the operation of space equipment[12]. Thus, study of the damage mechanism in those III-V compound semiconductor materials is essentially important for protecting the space equipment.

InAlAs/InGaAs material system is a typical III-V compound semiconductor, which possesses super transport characteristics and is widely applied for HEMT, SBD, and other devices[13-15]. Among them, InAlAs/InGaAs HEMT exhibits much lower noise figure and higher frequency performance which makes it suitable to apply in high-speed space communication system[16]. Ajayan et al. has reported a method to produce the InAlAs/InGaAs HEMT with 20 nm gate length, indicating that the maximum frequency f_{max} is up to 1460 GHz[17]. Up to know, however, most researchers always focus on the improving the work frequency whereas few people concentrate on investigating the irradiation process between ions and InAlAs/InGaAs materials. In order to better enable devices in space applications, it is highly desirable to explore the irradiation effects of the heavy ions onthose materials.

In this paper, the damage mechanism of the low energy He ion on the InAlAs and InGaAs is studied by Monte Carlo simulation. The effects of incidence energies and angles are discussed. Our research contributes to promote the III-V compound semiconductor devices applying in space environment.

2. Simulations

The irradiation effects of the He ion on InAlAs and InGaAs are studied by SRIM/TRIM packages. Interaction between the ions and the target material is described by binary-collision approximation[18]. The motion of the ions in the simulation is regarded as a series of independent collisions on the atoms, and each independent collision scattering is solved by numerical integration. The projected range, energy deposition and other parameters can be obtained from the SRIM package, by adoptings binary-collision approximation. In addition, the ion trajectory in the target can be imaged by the TRIM program[19,20]. The recoil of atoms, vacancies, and sputtering a can also be obtained.

In the simulation, the “Detailed Calculation with full Damage Cascades” mode has been selected to investigate the damage of the InAlAs and InGaAs induced by He ion irradiation. Energies and angles of the incident He ions are selected with the range from 50 keV to 180 keVand from 0^o to 89.9^o, respectively. Thickness of InAlAs and InGaAs are 2 μm. Density,

displacement energy, and other parameters of the InAlAs and InGaAs are shown in Table 1. Total number of the incident He ions is set to 10^4 in each simulation.

Table 1. Parameters of the $In_{0.52}Al_{0.48}As$ and $In_{0.53}Ga_{0.47}As$ materials in this simulation[21].

	$In_{0.52}Al_{0.48}As$	$In_{0.53}Ga_{0.47}As$
Mass density (g/cm3)	5.409	5.48
Thickness(um)	2	2
Surface binding energy (eV)	In:2.45 Al:3.36 As:1.26	In:2.45 Ga:2.82 As:1.26
Lattice binding energy (eV)	In:3 Al:3 As:3	In:3 Al:3 As:3
Displacement energy (eV)	In:6.7 Al:24 As:10	In:6.7 Ga:10 As:10

3. Results and discussion

Due to energy transfer to the target materials, the velocity of incidence ions gradually slows down, and ultimately stop at a certain depth in the material[22]. The He ion distributions in the InAlAs and InGaAs with different incident energies are shown in Fig. 1 (a) and (b). It can be seen from Fig. 1 that the peak position moves to deeper depth with increasing incident energy. Such a phenomenon is reasonable because the penetration ability of the He ion gradually enhances following the increasing incident. In addition, we also find that the He ions prefer to distribute near the peak position and conform to Bragg distribution.

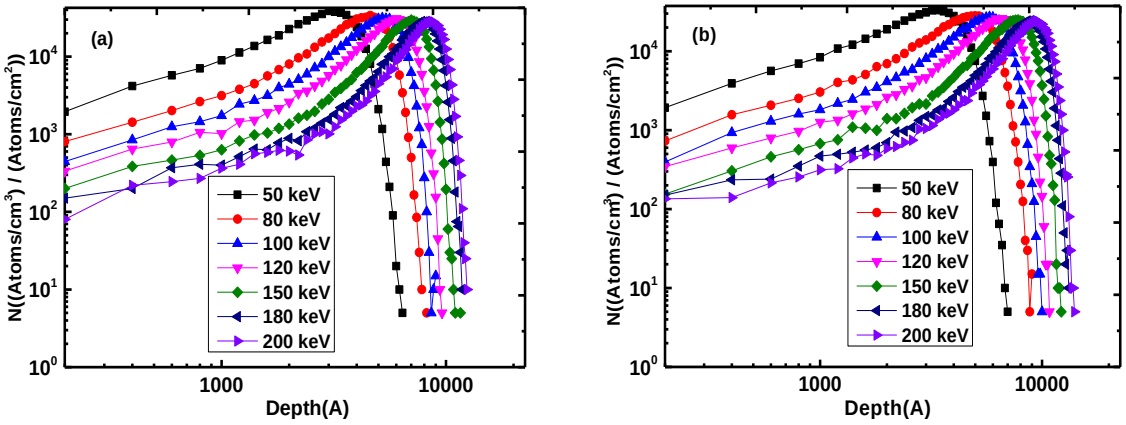

Fig. 1. Distribution of the He ions in InAlAs (a) and InGaAs (b) with different incident energies.

Projected range of the He ion in InAlAs and InGaAs with different incident energies is shown in Fig. 2. It can be seen that the projected ranges of both InAlAs and InGaAs grow up as the energy is increased from 50 keV to 200 keV. Moreover, the projected range for InGaAs is higher than that for InAlAs in the whole studied incident energies. This is mainly due to the displacement energy of the Al atom is much higher than that of the Ga atom, implying that the Al

atoms absorb more energy from the incident ions than the Ga atom for the same incident energy. Thus, InAlAs slows the velocity of ions

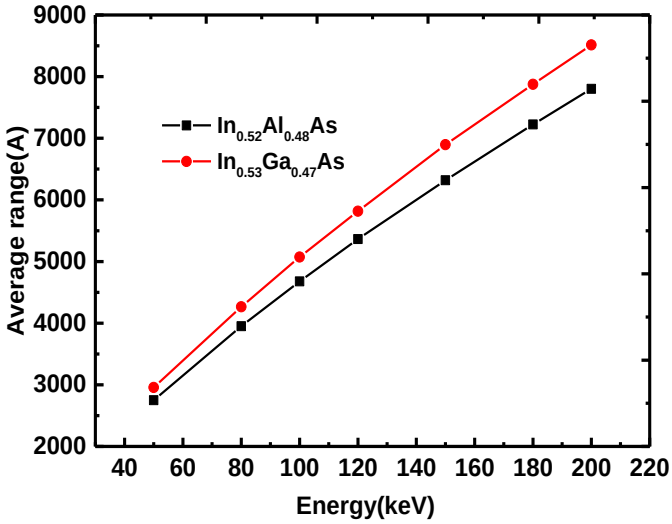

Fig. 2. Projected range of the He ions in InAlAs and InGaAs with different energies.

Figure 3 and 4 present the ionizing energy loss induced by He ion and recoil atom in InAlAs and InGaAs for different energies. The ionizing energy loss directly caused by the He ion is two orders of magnitude greater than that of the recoil atom for both InAlAs and InGaAs, and the distribution also moves to deeper depth with increasing incident energy. However, the incident depth dependent distributions of the ionizing energy loss induced by He ion and recoil atom show different behaviors. The distribution of ionizing energy loss induced by He ion is almost constant at lower depth and then rapidly drops, whereas that induced by recoil-atom conforms to Bragg distribution. Such a phenomenon is because that the ionizing energy loss directly caused by He ion mainly occurs in the proton transport process and drops sharply at the end of the He ion path, while that caused by recoil atoms mainly depends on the deposition position of the protons in the target.

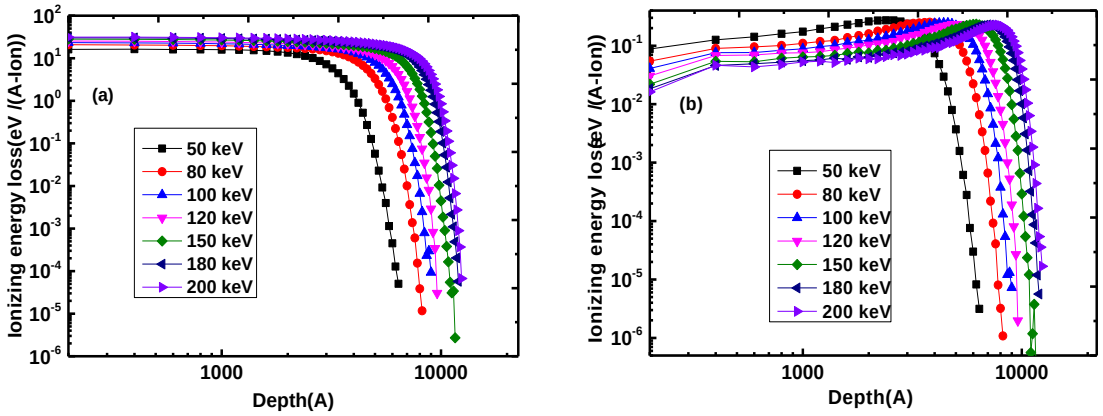

Fig. 3. Ionizing energy loss of InAlAs caused by (a) He ion and (b) recoil atom.

Hence, the peak position is near the projected range and also satisfies the Bragg peak distribution. In addition, we also notice that the ionizing energy loss of the InAlAs is slightly higher than that of the InGaAs.

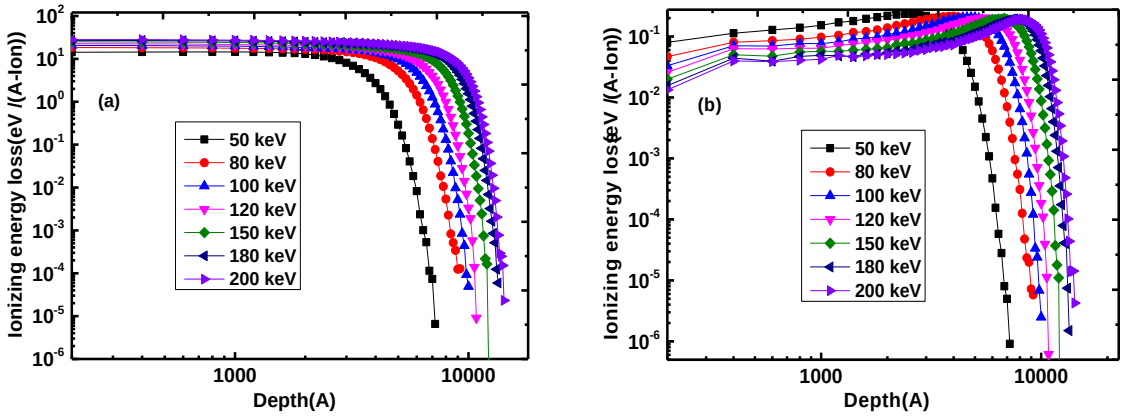

Fig. 4. Ionizing energy loss of InGaAs caused by (a) He ion and (b) recoil atom.

In addition to the ionizing energy loss, influence of the non-ionizing energy loss cannot be ignored. When He ions with different energies incident into the material, displacement damage will occur accompanied by the generation of irreversible vacancy defects in the material. Figures 5 and 6 show the relationship of vacancy defects with the target depth for $In_{0.52}Al_{0.48}As$ and $In_{0.53}Ga_{0.47}As$ at different energies. As can be seen from the figures, the distribution of the vacancy defects produced by He ion in the two materials is almost similar, which has a modest growth till reaches a summit and then rapidly falls with further depth increasing. This is because that the energy of the He ions gently decreases with penetrating into the deeper depth, whereas the As He ions penetrate deeper and deeper into the material, its energy slowly decreases, the nuclear stopping power gradually increases, and then reaches a peak. On the other hand, part of He ions will stop in the material, which will lead to a gradual decrease in the number of vacancies. Therefore, the change of vacancy with incident depth is the trend of increasing first and then decreasing.

Energy dependences of the vacancy numbers for each atom and total vacancies are shown in Figures 5(d) and 6(d). The vacancy numbers increase with increasing of energy. This is because that the projected range of the ions enlarges with energy, resulting in the gradual increase of the collision probability among ions and target atoms. It also can be seen from these two Figures that different atoms in one material show distinctive vacancy numbers and the As vacancy is always prominent.

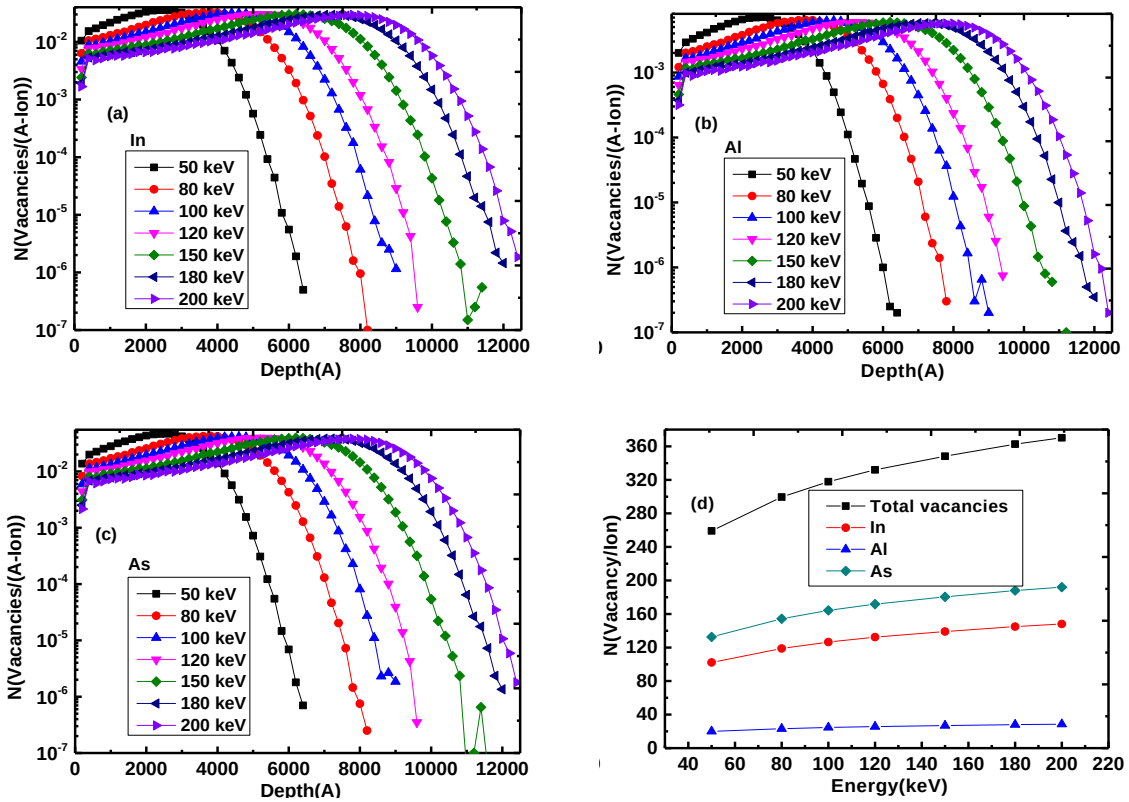

Fig. 5. Distribution of In vacancy (a), Al vacancy (b), As vacancy (c), and total vacancies (d) for InAlAs.

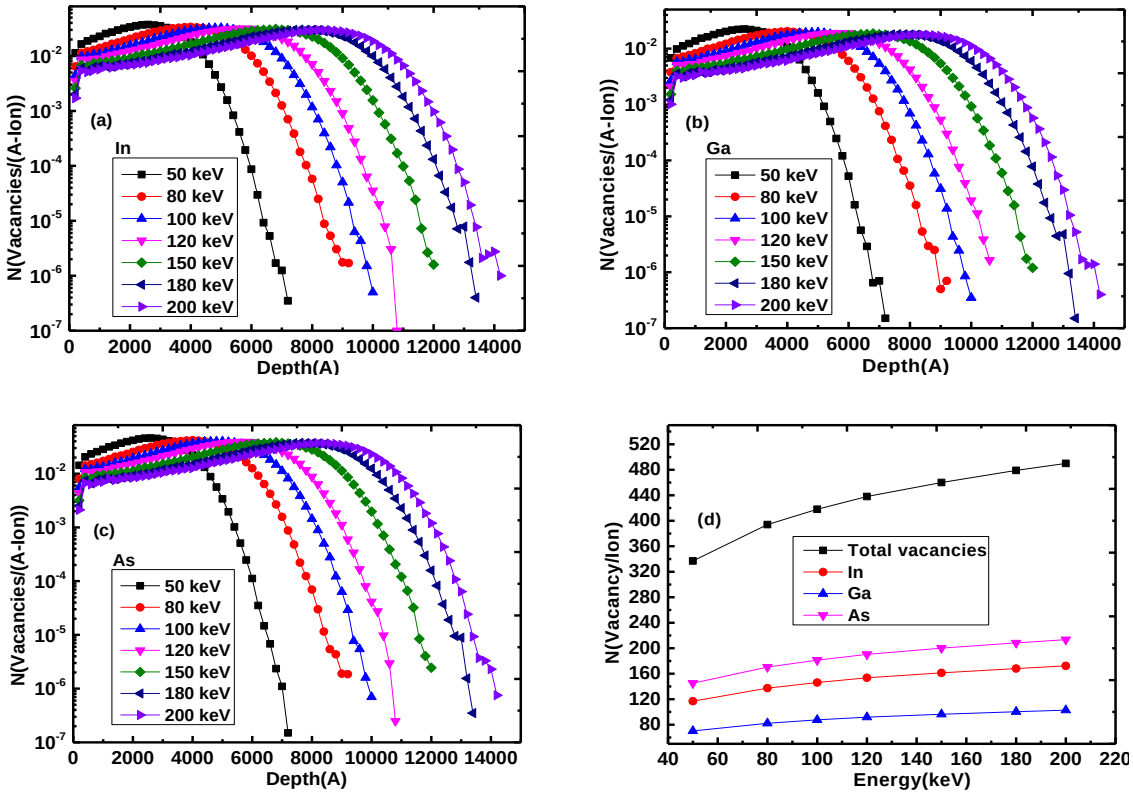

Fig. 6. Distribution of In vacancy (a), Al vacancy (b), As vacancy (c), and total vacancies (d) for InGaAs.

Figures 7 and 8 show the phonons distribution in InAlAs and InGaAs versus the depth at different energies. They show almost similar tendencies with depth. In addition, the phonon number induced by recoil atoms is much higher than that induced by He ions. Energy required for phonon production is very low and mainly distributes at the end of the path, but phonons are vibrations of the atoms themselves, so recoil atoms should produce more phonons than protons for the same energy.

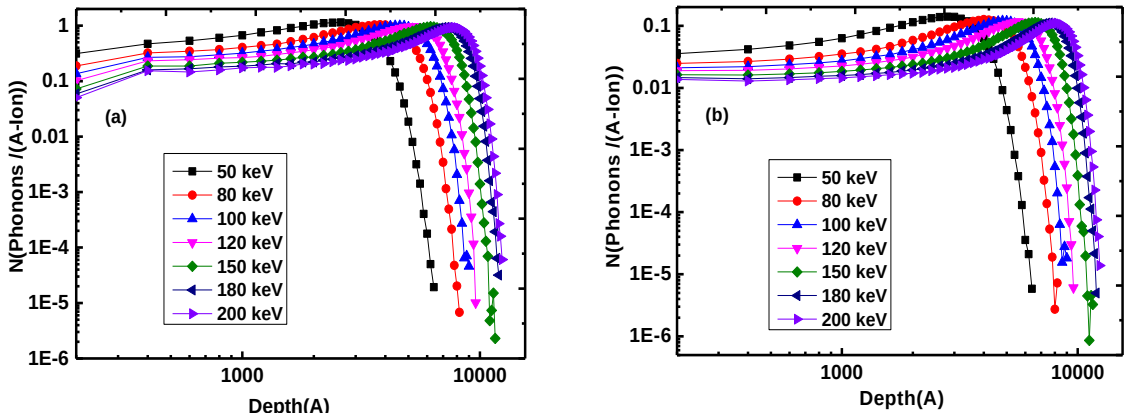

Fig. 7. Phonon distribution for recoil atoms (a) and He ions (b) in InAlAs versus the depth at different energies.

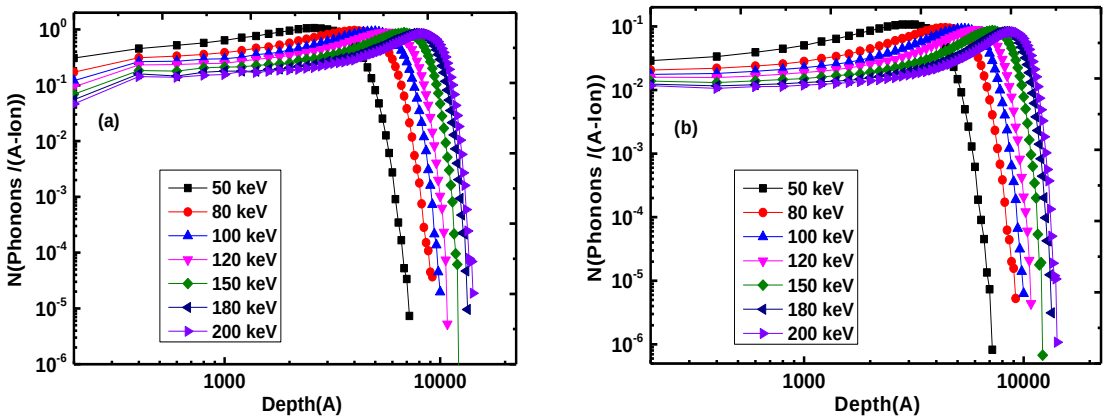

Fig. 8. Phonons distribution for recoil atoms (a) and He ions (b) in InGaAs versus the depth at different energies.

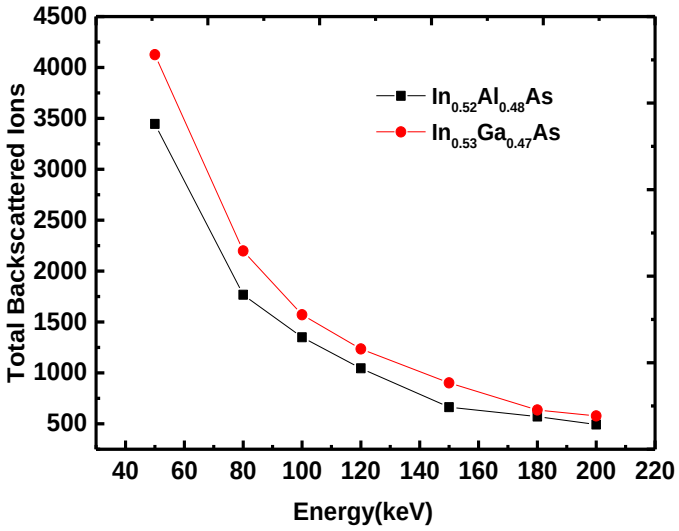

Fig. 9. Backscattering ion number for InAlAs and InGaAs at different energies.

Figure 9 shows the total numbers of the backscattering ions for InAlAs and InGaAs with the energies ranging from 50 to 200 keV. They all decline with increasing energy for these two materials. Also, the number of the backscattering ions for InAlAs is always higher than that for InGaAs in the whole studied energy range. At high energies, the ions travel deeper in materials and transfer more energies to the atoms far away from the surface of the material. In this case, the ions cannot obtain enough energy to escape from the surrounding atomic potential field, resulting in the decrease of the backscattering ion number at high energies.

4. Conclusions

In conclusion, influence of the He ions irradiations with different energies on InAlAs and InGaAs is comprehensively explored, including the He ion distribution, ionizing energy loss distribution, vacancies distribution and backscattering ion number. Our results show that the peak position of He ion distribution moves to deeper depth with increasing incidence energy and the distribution curve conforms to Bragg distribution. For both the InAlAs and InGaAs, the distribution of ionizing energy loss, induced by He ions is two orders of magnitude greater than that of the recoil atoms.

In addition, the former is almost constant first and then shows a sharp drop at high energies, while the latter conforms to Bragg distribution. The number of the vacancy first modestly increases and then declines rapidly with the increasing depth. It also increases with increasing energy and the As vacancy are dominating vacancy for two materials. The number of phonons induced by recoil atoms is much higher than that induced by He ions. The total numbers of the backscattering ions for these two materials all decline with increasing erengy and the value of the InGaAs is always higher than that of the InAlAs.

Acknowledgements

This research was funded by the Project funded by China Postdoctoral Science Foundation (No.2021M700685), Key Scientific Research Projects of Colleges and Universities in Henan Province (No.21B140006, 22A510016), Henan Provincial Science and Technology Research Project (222102310286) National Scientific Research Project Cultivation Fund of Huanghuai University (No. XKPY-202103, XKPY-202106, XKPY-202006), the Award Plan for Tianzhong Scholars of Huanghuai University in 2019, Henan Provincial Key Laboratory of Smart Lighting.

References

[1] S. J. Pearton, A. Aitkaliyeva, M. Xian, F. Ren, A. Khachatrian, A. Ildefonso, Z. Islam, M. A. Jafar Rasel, A. Haque, A. Y. Polyakov, J. Kim, ECS Journal of Solid State Science and Technology, 10, 055008(2021); https://doi.org/10.1149/2162-8777/abfc23

[2] S. X. Sun, Y. H. Zhong, H. Y. Mei, R. X. Yao, F. J. Chen, Y. X. Li, Y. F. Hu, Journal of Ovonic Research, 17(2), 137-145(2021).

[3] H. Elmir, B. Dennai, M. Fillali, Journal of Ovonic Research, 17(3), 307-311(2021).

[4] Y. Chen, L. A. Yang, Z. Jin, Y. B. Su, Y. Hao, IEEE Transactions on Electron Devices, 68(5), 2226(2021); https://doi.org/10.1109/TED.2021.3066139

[5] W. He, J. Li, Z. L. Liao, F. Lin, J. Y. Wu, B. Wang, M. J. Wang, N. Liu, H. C. Chiu, H. C. Kuo, X. N. Lin, J. B. Li, X. K. Lin, Nano Express, 17, 14(2022); https://doi.org/10.1186/s11671-022-03653-z

[6] N. Jankovic, S. Faramehr, P. Igic, Journal of Computeational Electronics, 21, 191-196(2022); https://doi.org/10.1007/s10825-021-01835-z

[7] M. W. Ha, D. W. Hwang, C. K. Hahn, Y. S. Kim, Journal of the Korean Physical Society, 60, 1629-1633(2012); https://doi.org/10.3938/jkps.60.1629

[8] X. Mei, W. Yoshida, M. Lange, J. Lee, J. Zhou, P. H. Liu, K. Leong, A. Zamora, J. Padilla, S. Sarkozy, R Lai, W. R. Deal 2015 IEEE Electron Devices Letters, 36, 327(2015); https://doi.org/10.1109/LED.2015.2407193

[9] S. X. Sun, X. L. Fu, L. Wang, M. E, J. J. Yi, R. X. Yao, X. Y. Zheng, H. T. Wu, F Liu, Y. H. Zhong, Y. X. Li, P. Ding, Z. Jin, Journal of Ovonic Research, 17(5), 411-420(2021).

[10] S. X. Sun, P. Ding, Z. Jin, Y. H. Zhong, Y. X. Li, Z. C. Wei, Nanomaterials, 9, 967(2019); https://doi.org/10.3390/nano9070967

[11] B. Yang, J. J. Zhang, S. X. Sun, Y. N. Jin, X. Q. Zhao, S. H. Meng, Y. F. Hu, Y. H. Zhong, Z. Jin, Nuclear Inst. and Methods in Physics Research B, 484, 42-47(2021); https://doi.org/10.1016/j.nimb.2020.09.024

[12] H. Y. Mei, H. T. Wu, R. X. Yao, L. Y. Zhao, X. Y. Zheng, F. Liua, I. H. Wen, S. X. Sun, Digest Journal of Nanomaterials and Biostructures, 17(1), 39-46(2022).

[13] Z. H. Tong, P. Ding, Y. B. Su, D. H. Wang, Z. Jin, Chinese Physics B, 30(1), 018501(2021); https://doi.org/10.1088/1674-1056/abb30d

[14] C. H. Lai, T. Y. Lee, J. S. Huang, K. W. Lee, Y. H. Wang, Materials Science in Semiconductor Processing, 129, 105804(2021); https://doi.org/10.1016/j.mssp.2021.105804

[15] J. Ajayan, D. Nirmal, R. Mathew, D. Kurian, P. Mohankumar, L. Arivazhagan, D. Ajitha, Materials Science in Semiconductor Processing, 128, 105753(2021); https://doi.org/10.1016/j.mssp.2021.105753

[16] J. Ajayan, D. Nirmal, R. Mathew, D. Kurian, P. Mohankumar, L. Arivazhagan, D. Ajitha, Materials Science in Semiconductor Processing, 128, 105753(2021); https://doi.org/10.1016/j.mssp.2021.105753

[17] J. Ajayan, T. Ravichandran, P. Prajoon, J. Charles Pravin, D. Nirmal, Journal of Computational Electronics, 17, 265-272(2018); https://doi.org/10.1007/s10825-017-1086-4

[18] S. X. Sun, Y. H. Zhong, R. X. Yao, F. J. Cen, Y. X. Li, Digest Journal of Nanomaterials and Biostructures, 15(4), 1089-1095(2020).

[19] N. Dahbi, R. B. Taleb, O. Zaoui, Journal of Ovonic Research, 15(3), 167-172(2019); https://doi.org/10.54648/AIAJ2019011

[20] D. Nath, R. Das, Vacuum, 190, 110293(2021); https://doi.org/10.1016/j.vacuum.2021.110293

[21] X. H. Zhao, H. L. Lu, Y. M. Zhang, Y. M. Zhang, Microelectronics Reliability, 78, 156-160(2017); https://doi.org/10.1016/j.microrel.2017.07.097

[22] M. El Marsi, R. Moultif, S. Lahlou, S. Rochd, A. Dezairi, Nuclear Instruments and Methods in Physics Research B, 430, 72-78(2018); https://doi.org/10.1016/j.nimb.2018.05.046